IEEE Access
Multidisciplinary | Rapid Review | Open Access Journal

Received 11 July 2023, accepted 26 July 2023, date of publication 3 August 2023, date of current version 10 August 2023.

Digital Object Identifier 10.1109/ACCESS.2023.3301850

RESEARCH ARTICLE

Resonant Frequency Tracking Scheme for *LLC* Converter Based on Large and Small Signal Combined Model

RUNHUI HE, (Student Member, IEEE), BO XUE, (Student Member, IEEE), MINGDE ZHOU, (Student Member, IEEE), MINFAN FU, (Senior Member, IEEE), JUNRUI LIANG, (Senior Member, IEEE), YU LIU, (Senior Member, IEEE), AND HAOYU WANG, (Senior Member, IEEE)

School of Information Science and Technology, ShanghaiTech University, Shanghai 201210, China

Corresponding author: Haoyu Wang (wanghy@shanghaitech.edu.cn)

This work was supported in part by the National Natural Science Foundation of China under Grant 52077140, and in part by the Shanghai Rising Star Program under Grant 20QA1406700.

ABSTRACT To achieve optimal system performance, it's recommended to operate an *LLC* resonant converter at its resonant frequency. However, in mass production, the resonant parameters of different products can deviate significantly. This means that we need to actively track the resonant frequency during practical usage. To address this issue, this paper presents a novel automatic control scheme for *LLC* converter that tracks the resonant frequency. The proposed control scheme is based on an accurate small-signal model, and an extended state observer which provides small-signal characteristics at the operating frequency. The controller checks the voltage gain of the converter and combines large-signal with small-signal models to control the *LLC* converter effectively. Compared to conventional automatic resonant frequency tracking (ARFT) control schemes, the proposed control scheme is easier to implement and requires fewer sensors. Experimental results demonstrate its effectiveness in tracking the resonant frequency. In summary, this manuscript proposes an effective ARFT control scheme for *LLC* converter that can track the resonant frequency with reduced sensors and is easier to implement.

INDEX TERMS Automatic resonant frequency tracking (ARFT), dc–dc converter, extended state observer (ESO), *LLC* resonant converter, small-signal model.

I. INTRODUCTION

L*LC* resonant converters is a widely used isolated dc/dc topology due to its primary-side zero-voltage switching (ZVS) and secondary-side zero-current switching (ZCS) [1], [2], which leads to high efficiency and power density, The schematic of full bridge *LLC* converter is shown in Fig. 1.

One of the key advantages of *LLC* converter is its high efficiency. With the help of wide band gap semiconductor devices and soft switching characteristics, the operating frequency can be pushed to high frequency range while still maintain high efficiency [3]. Under such high operating frequency, the volume of *LLC* converters can be greatly reduced, which facilitates a compact system integration [4].

There are some limitations of *LLC* converters. On one hand, for *LLC*-based dc transformers (DCX), the operation of the resonant converters is confined at its resonant frequency. However, in massive production scenarios, it is frequent to encounter parameter mismatches. While *LLC* converters are sensitive to resonant parameter deviations [5]. This leads to the shift of resonant frequency, which results in a high MOSFET turn-OFF current and a large circulating current. Moreover, the voltage gain and efficiency would also be affected [6]. On the other hand, *LLC* converters exhibit non-linear characteristics [7]. The voltage gain depends on parameters of the controller and resonant circuit, which results in non-linear

The associate editor coordinating the review of this manuscript and approving it for publication was Kan Liu.

This work is licensed under a Creative Commons Attribution-NonCommercial-NoDerivatives 4.0 License.
For more information, see https://creativecommons.org/licenses/by-nc-nd/4.0/

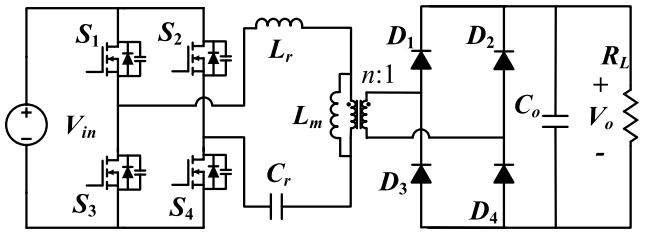

FIGURE 1. Schematic of full-bridge *LLC* resonant converter.

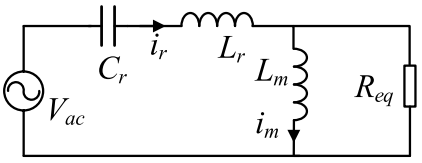

FIGURE 2. Equivalent circuit model of full-bridge *LLC* resonant converter.

behavior. The non-linear behavior can cause harmonic distortion and voltage overshoot, which poses high difficulty in prediction and control, whereas traditional control methods exhibit poor performance [8].

To address these issues, different control and modulation techniques are investigated, to improve the linearity of the converter and reduce the impact of non-linear behavior [9]. Normally, the *LLC* converter operates in the vicinity of its resonant frequency to achieve the optimal efficiency and unity normalized gain, and the simplest method is based on frequency modulation [10].

State-of-the-art control strategies for *LLC* converter can be divided into two categories: large-signal model based strategies and small-signal model based strategies, also there are many other control or modulation strategies [11].

The first category is based on the small-signal model. In [12], a unified automatic resonant frequency tracking (ARFT) scheme is established based on the gain or phase relationship between different variable pairs in resonant tank. This method exhibits high tracking accuracy. In [13], a small-signal model for series resonant converter is investigated considering phase-shift and switching frequency as the control parameters, a compensator is inserted into the control loop to improve the dynamic response of resonant converters. However, to detect both the phase and gain relationship, the hardware cost is high and requires a lot of computing time.

The second category is based on large-signal model. The relationship of variables in resonant tank and output voltage is utilized to track the resonant frequency. In [14], a simple ARFT scheme is proposed based on the gain relationship between the *LLC* resonant converter output and input voltages. In [15], a method that detect the phase difference of two sides of the transformer is proposed to ensure CLLC converters can always work at maximum efficiency point in both forward and backward modes even under resonant tank parameter deviations. To ensure ZVS operation, a multi-variable switching frequency-duty cycle hybrid control strategy is presented for *LLC* converter [16]. Although the above mentioned methods maintain low cost and control circuit loss, the tracking performance is not optimal due to the non-linear characteristics of *LLC* resonant converter.

Time durations related to resonant frequency, such as the zero-current duration of the secondary side diode, can be used to control the *LLC* converter [17]. This is because it has a linear relationship with the resonant frequency and is independent of resonant circuit parameters. However, this method can't work if the switching frequency is higher than the resonant frequency, as this mode no longer exists. In [18] a method is developed to detect the zero-crossing point and peak point of resonant current. The duration between those two points is a quarter of the resonant period. This method is simple and doesn't need prior knowledge of resonant frequency. However, almost all the time-duration-based methods require additional current sensors and zero current detection. This increases the hardware cost of the ARFT scheme. Hence, an ARFT scheme with easily implementation and high tracking accuracy is required.

For conventional *LLC* resonant converter, observer-based controller outperforms PID controller better in dynamic response and static accuracy [19]. This concept can be extended to ARFT scheme. Extended state observer (ESO) is considered one of the most suitable controller to estimate uncertainties [20], which gains its popularity in ARFT techniques for *LLC* resonant converter. ESO treats unknown dynamics and the external disturbance as a total disturbance f, in which f can be used to predict the resonant frequency of *LLC* resonant tank. ESO-based ARFT scheme has advantages in both cost and tracking accuracy. In [21], a second-order *LLC* converter small-signal model is presented using the extended describing function (EDF) method with a simplified resonant circuit. Accordingly, a new adaptive scheme that automatically updates the inner model of extended state observer is proposed.

To this end, in this manuscript, a novel ARFT controller based on extended state observer and voltage gain difference is proposed for *LLC* resonant converter. This manuscript is a further extension of the conference paper [21]. The ARFT control scheme inherits the previous small-signal tracking method but expands it to combine both large-signal and small-signal approaches. The controller By combining these two approaches, the ARFT control scheme can provide robust and accurate control of the *LLC* converter.

This manuscript is organized as follows: Section II introduces the large-signal model and small-signal model of *LLC* resonant converter. Section III demonstrates the ARFT control scheme and the detailed controller design. Then, Section IV provide the experiment results. Finally, the manuscript concludes in Section V.

II. ANALYSIS OF THE *LLC* RESONANT CONVERTER

LLC resonant converter, as shown in Fig. 1, can be analyzed from the perspective of impedance. Its equivalent circuit model is plotted in Fig. 2. The inverter bridge can be modeled as an ac voltage source by only considering the fundamental frequency component V_{ac}. The resonant circuit part is retained, the rectifier bridge can be regarded as an ac equivalent resistance.

Under this perspective, the voltage gain of full-bridge *LLC* resonant converter can be exported as:

$$G_{V_i} = \frac{1}{n\sqrt{(Qf_n(1-f_n^{-2}))^2 + (1+L_n-L_nf_n^{-2})^2}}. \quad (1)$$

where Q is the quality factor which is related to load and relative inductance, L_n is the ratio of L_m and L_r:

$$Q = \frac{\sqrt{L_r/C_r}}{R_{eq}}, \quad L_n = \frac{L_m}{L_r}. \quad (2)$$

The gain curve versus switching frequency under different load condition of *LLC* resonant converter is plotted in Fig. 3. It can be seen that all gain curves intersect at the unity gain point at the resonant frequency f_r.

The simplest way to extract resonant frequency is by numerically inverting the voltage gain expression (1). However, it is difficult to solve since there are many unknowns such as transformer magnetizing inductance L_m and resonant tank parameters. Due to this non-linear behavior, controlling *LLC* converter purely from the aspect of large-signal is difficult work.

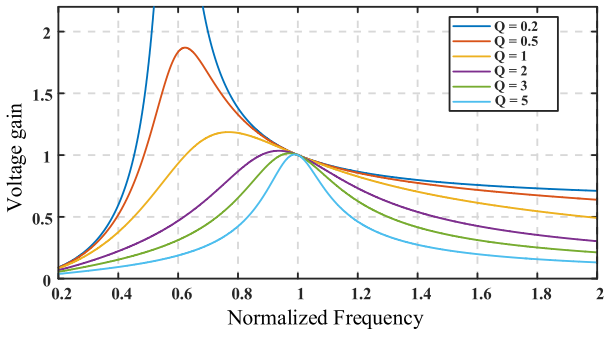

FIGURE 3. The gain curve of *LLC* resonant converter.

We can turn our attention to small signal methods for help. An accurate small-signal model of the *LLC* resonant converter is required to build ESO control scheme. The volt-frequency characteristic of *LLC* resonant converter is nonlinear, which make it difficult to derive the model. To address this issue, the extended describing function (EDF) method is adopted. By applying the Kirchhoff's laws to four state variables (The resonant currents i_r, i_m, the resonant voltage v_{cr} and the output capacitor voltage v_{Co}) which can characterize *LLC* resonant converter, we can obtain:

$$\begin{cases} \dfrac{di_r}{dt} = \dfrac{v_{in} - v_{cr} - \mathrm{sgn}(i_r - i_m)nv_{Co}}{L_r} \\ \dfrac{dv_{cr}}{dt} = \dfrac{i_r}{C_r} \\ \dfrac{di_m}{dt} = \dfrac{nv_{Co}\mathrm{sgn}(i_r - i_m)}{L_m} \\ \dfrac{dv_{Co}}{dt} = \dfrac{n|i_r - i_m|}{C_o} - \dfrac{v_{Co}}{R_L}. \end{cases} \quad (3)$$

where R_L is the load resistance and C_o is the output capacitance.

When the *LLC* resonant converter works at a steady state, the waveforms of four state variables are nearly sinusoidal. Based on first harmonic approximation, we can rewrite (3), where ω_s is the switching angular frequency:

$$\begin{cases} i_r(t) = i_{rs}\sin\omega_s t + i_{rc}\cos\omega_s t \\ v_{cr}(t) = v_{cs}\sin\omega_s t + v_{cc}\cos\omega_s t \\ i_m(t) = i_{ms}\sin\omega_s t + i_{mc}\cos\omega_s t \\ v_{Co}(t) = v_{Cos}\sin\omega_s t + v_{Coc}\cos\omega_s t. \end{cases} \quad (4)$$

Each of the four steady-state variables has sin part and cos part under sinusoidal approximation, and their values are denoted in the subscript as "s" or "c".

Applying Fourier expansions to the nonlinear terms, the EDF method can be used to approximate *LLC* resonant converter model. The EDFs are defined as (5) [19]:

$$\begin{cases} f_1(v_{in}, d) = \dfrac{4}{\pi}v_{dc} \\ f_2(i_{rs} - i_{ms}, i_p, V_{Co}) = \dfrac{4}{\pi}\dfrac{i_{rs} - i_{ms}}{i_p}v_{Co} \\ f_3(i_{rc} - i_{mc}, i_p, V_{Co}) = \dfrac{4}{\pi}\dfrac{i_{rc} - i_{mc}}{i_p}v_{Co} \\ f_4(i_{rs} - i_{ms}, i_{rc} - i_{mc}) = \dfrac{2}{\pi}i_p. \end{cases} \quad (5)$$

where i_p is the peak current of the resonant inductor and can be expressed as

$$i_p = \sqrt{(i_{rs} - i_{ms})^2 + (i_{rc} - i_{mc})^2}. \quad (6)$$

Substituting EDFs into (3), we can obtain an equivalent circuit model of *LLC* resonant converter. However, the order of this model is too high. Thus, some approximation should be adopted. The resonant circuit can be simplified as the capacitor behaves like an equivalent inductor concerning the small-signal beat frequency [22]:

$$L_e = L_r + \frac{1}{C_r\omega_s^2} = L_r(1 + \frac{\omega_r^2}{\omega_s^2}). \quad (7)$$

where ω_r is the resonant angular frequency.

After perturbing the small-signal quantities, we can linearize the LLC converter and obtain its small-signal model. This model separates the resonant tank into sine part and cosine part, as depicted in Fig. 4.

In this model, we consider the current of rectifier circuit as i_{Tc} and i_{Ts}, which also can be expressed as:

$$i_{Tc} = i_{rc} - i_{mc}. \tag{8}$$

$$i_{Ts} = i_{rs} - i_{ms}. \tag{9}$$

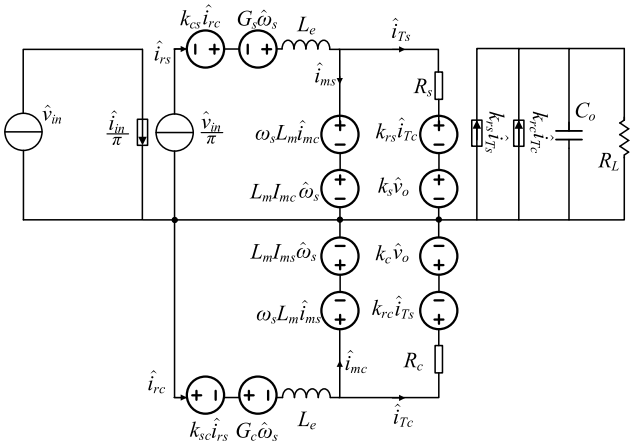

FIGURE 4. Separated equivalent small-signal model of *LLC* resonant converter.

Then, a second-order transfer function between the output voltage and the switching frequency at the resonant frequency is obtained:

$$\frac{V_o}{\omega_s} = G_{DC}\frac{1}{1 + \frac{s}{Q_p\omega_p} + (\frac{s^2}{\omega_p^2})}. \tag{10}$$

where

$$Q_p = \frac{8n}{\pi^2}R_L\sqrt{\frac{C_o}{L_e}}, \quad \omega_p = \sqrt{\frac{8n}{L_e\pi^2 C_o}}. \tag{11}$$

G_{DC} is the slope of the dc gain of the control-to-output voltage transfer function. G_{DC} can be related to the slope of the voltage gain curve plotted in Fig.3 by the relation shown in the following equation:

$$G_{DC} = \frac{\partial V_o}{\partial \omega_s} = \frac{V_{in}}{n\omega_s}\frac{\partial G_{Vi}}{\partial \omega_s} \tag{12}$$

This relationship between the output voltage and switching frequency can be rewritten as:

$$\ddot{V}_o = -\frac{\omega_p}{Q_p}\dot{V}_o - \omega_p^2 V_o + G_{DC}\omega_p^2\omega_s = h(V_o, \omega_s). \tag{13}$$

This transfer function will be used in designing the ESO and improving the control accuracy.

III. PROPOSED ARFT SCHEME BASED ON EXTENDED STATE OBSERVER

By combining the large-signal and small-signal models, the proposed controller can be obtained. Its flowchart is plotted in Fig. 5. For the extended state observer, the input is the converter output voltage ripple and switching frequency. For the large-signal part, the input is the converter voltage gain. First,the controller checks the voltage gain of the converter, if the deviation is greater than the threshold ΔG_{th}, there will be a variation ΔF_s added into the control variable f_s. In this process, large-singal PI controller provides ΔF_{s1}, and the extended state observer provides a variation ΔF_{s2} based on the small-signal model of *LLC* converter, the sum of them is ΔF_s. Then the controller generate the switching frequency according to calculation, to form the driving signal of the *LLC* converter.

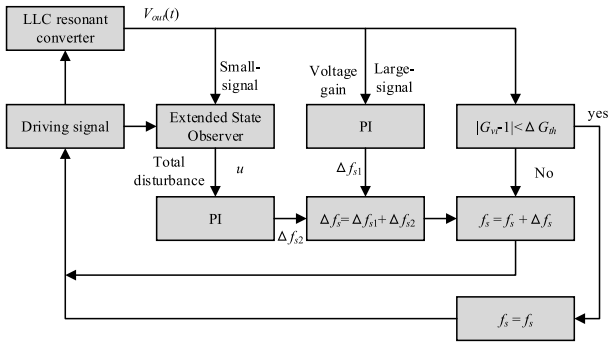

FIGURE 5. Flowchart of the proposed controller.

Firstly, we need to construct an observer to obtain the output voltage of *LLC* converter. The ESO considers the internal uncertainties and external disturbances as the total disturbance f, so we can rewrite equation (13):

$$\ddot{V}_o = -\frac{\omega_p}{Q_p}\dot{V}_o - \omega_p^2 V_o + (b - b_0)\omega_s + b_0\omega_s = f + b_0\omega_s. \tag{14}$$

where

$$f = -\frac{\omega_p}{Q_p}\dot{V}_o - \omega_p^2 V_o + (b - b_0)\omega_s$$
$$b_0 = \frac{-8V_{in}}{\pi}\frac{L_n}{\omega_s}\frac{n}{L_r C_o}. \tag{15}$$

b_0 is set as the value when equation (12) under the optimal operating point $\omega_s = \omega_r$, and b is the coefficient of ω_s.

Define the state as $x = [x_1, x_2, x_3]^T = [V_o, \dot{V}_o, f]^T$, thus an extended state-space matrix can be derived as(16):

$$\begin{cases} \dot{x} &= Ax + Bu + E\dot{f} \\ y &= Cx. \end{cases} \tag{16}$$

where

$$A = \begin{bmatrix} 0 & 1 & 0 \\ 0 & 0 & 1 \\ 0 & 0 & 0 \end{bmatrix}, B = \begin{bmatrix} 0 \\ b_0 \\ 0 \end{bmatrix}, E = \begin{bmatrix} 0 \\ 0 \\ 1 \end{bmatrix}, C = \begin{bmatrix} 1 & 0 & 0 \end{bmatrix}. \tag{17}$$

To deploy the ESO experimentally, it needs to be discretized by sampling with the sampling period T_s. According to the zero-order hold (ZOH) properties, it can be obtained from (16) that $x(k) = x(kT_s)$, $u(k) = u(kT_s)$, $f(k) = f(kT_s)$, $y(k) = y(kT_s)$.

Then a discrete-time observer named ESO can be constructed [23]:

$$\begin{cases} \tilde{x}(k+1) = A\tilde{x}(k) + Bu(k) + L_o(y(k) - \tilde{y}(k)) \\ \tilde{y}(k) = C\tilde{x}(k). \end{cases} \tag{18}$$

where L_o is the observer gain, which is used to amplify the error between the observer values and the actual values, ensuring that the observer values closely approximate true values.

$$L_o = \begin{bmatrix} l_1 & l_2 & l_3 \end{bmatrix}^T. \tag{19}$$

$\tilde{x}(k), \tilde{y}(k)$ are the estimated value of $x(k), y(k)$ from ESO. Then the estimated dynamic error $e(k)$ of ESO is:

$$e(k+1) = Le(k) + bh(k). \tag{20}$$

where

$$L = \begin{bmatrix} -l_1 & 1 & 0 \\ -l_2 & 0 & 1 \\ -l_3 & 0 & 0 \end{bmatrix}, b = \begin{bmatrix} 0 \\ 0 \\ 1 \end{bmatrix}, e(k) = \begin{bmatrix} \tilde{x}_1(k) - x_1(k) \\ \tilde{x}_2(k) - x_2(k) \\ \tilde{x}_3(k) - x_3(k) \end{bmatrix}. \tag{21}$$

To make sure that L is asymptotically stable, L_o is tuned using the bandwidth method. This sets the characteristic polynomial of the observer to [24]:

$$z^3 + l_1 z^2 + l_2 z + l_3 = (z + \omega_o)^3. \tag{22}$$

It can be proved that when L is asymptotically stable, $\tilde{x}(k)$ approaches $x(k)$ and the observer error $e(k)$ converges to zero because we ensure that all eigenvalues are locating in the left half plane. As the observer value $\tilde{x}_3(k)$ close to the resonant frequency, we can use this predicted value to control the *LLC* converter. In our previous conference paper, when the switching frequency is near the resonant frequency, predicted resonant frequency maintain good accuracy [21].

After obtaining the estimated total disturbance, we can get the predicted resonant frequency:

$$u = \frac{u_0 - \tilde{f}}{b_0}. \tag{23}$$

where u_0 is reference of control input. Then, we can derive the final Δf_{s2} from using a PI controller based on the predicted resonant frequency:

$$\Delta f_{s2} = u(k_p + \frac{k_i}{s}). \tag{24}$$

The control transfer functions $G_{cl}(s)$ used for designing large-signal parts are diverse, and different transfer functions can have varying performances. To have a better comparison results, PI regulator is selected as $G_{cl}(s)$, and the parameters of $G_{cl}(s)$ are consistent with the situation where only the PI regulator is active for *LLC* converter.

IV. EXPERIMENTAL RESULTS

A. EXPERIMENT SETUP

LLC converters often encounter the issue of parameter mismatches. Specifically, when the switching frequency and the resonant frequency are not matched, it can lead to performance degradation. In our experiment, we intentionally created mismatched conditions to assess the capability of our algorithm in successfully compensating this mismatch. The purpose is to determine whether our algorithm could effectively address the negative effects resulting from such parameter mismatches.

TABLE 1. Parameters of the *LLC* converter prototype in experiment.

Symbol	Parameter	Value
V_{in}	Input voltage	20 V
V_{out}	Output voltage	20 V
L_r	Inductance of resonant inductor	33.8 μH
C_r	Capacitance of resonant capacitor	70 nF
C_r'	Switched resonant capacitor	21 nF
L_m	Inductance of magnetizing inductor	146 μH
n	Transformer ratio	1
R_L	Load resistance	20 Ω
f_{r1}	Resonant frequency 1	105 kHz
f_{r2}	Resonant frequency 2	91 kHz

In experimental verification, a hardware prototype is designed and tested. The ARFT control scheme proposed in Section IV is implemented in TMS320F28335. The *LLC* converter's output voltage is sensed by the ADC, and send to DSP calculates in real time. The detailed parameters of the prototype in the experiment are presented in Table 1.

The topology of experiment *LLC* converter is shown in Fig.6. Compared with the traditional *LLC* converter, there is an additional branch paralleled with the original resonant capacitor C_r. This branch consists of a switch and another resonant capacitor C_r'. A pair of back-to-back MOSFETs are employed as the four-quadrant switch. MOSFET output parasitic capacitor is denoted as C_{oss}. In turn-OFF mode, C_{oss} is in series with C_r', so the capacitance of switched resonant branch is almost equal to C_{oss}, which has little impact on the main resonant branch. While in turn-ON mode, the capacitance of switched resonant branch is C_r', the resonant capacitance of prototype changes to $C_r' + C_r$, which lead to the resonant frequency of *LLC* converter change form f_{r2} to f_{r1}. The experiment prototype can achieve a step change of resonant circuit parameters.

Fig. 7 shows the designed experimental prototype. DSP interface provides I/O ports for the controller to form the required frequency of *LLC* converter and generate the driving signals of the inverter bridge; the inverter bridge is

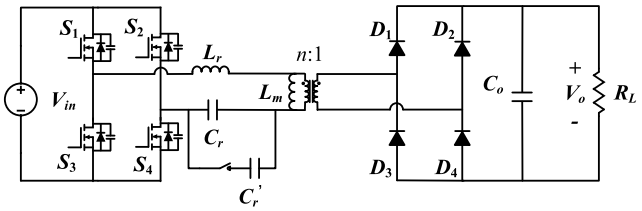

FIGURE 6. The topology of experiment *LLC* converter prototype.

built by MOSFETs, switched resonant branch consists of two back-to-back MOSFETs and a capacitor C_r'. When the four-quadrant switch is turn-ON, C_r' will access the resonant circuit, causing the sudden increase of the resonant capacitor. The same to the situation when four-quadrant switch is turn-OFF, the resonant capacitor suddenly drops.

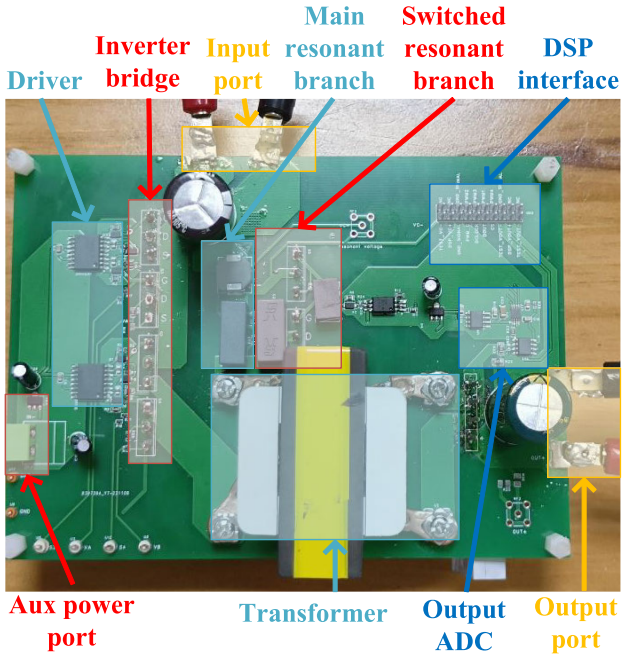

FIGURE 7. Experiment *LLC* converter prototype.

Fig. 8 gives the block diagram of the experiment control setup. The output ADC shown in Fig. 7 is selected as ADS8320, and then the data will be sent to controller, and finished the proposed control loop calculation.

Fig. 9 illustrates the open-loop dynamic response test conducted on our designed prototype. In the test, the resonant capacitor undergoes a step change from 70 nF to 91 nF. The step change in capacitance is initiated by activating the four-quadrant switch, which in turn affects the output voltage. As a results of this change, the resonant current deviates from a pure sinusoidal waveform and exhibits a slight distortion.

The zoomed version at capacitance sudden increase instant is shown in Fig. 10. The degree of resonant current overshoot is tolerable. The instant of C_r' access in should be better set to when the main branch capacitor voltage is 0, but it

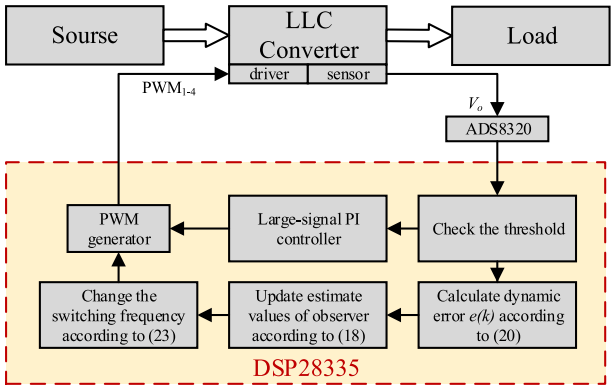

FIGURE 8. Block diagram of the experiment setup.

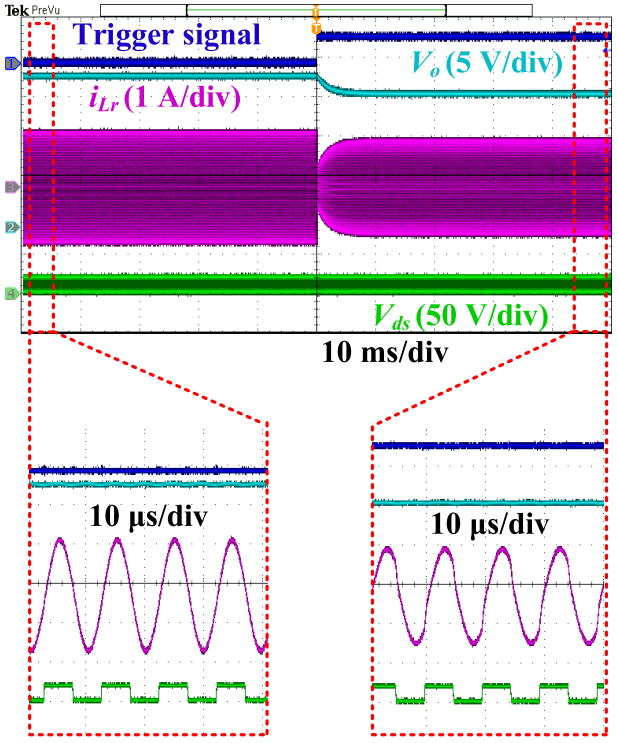

FIGURE 9. Experiment results of the prototype under resonant capacitor sudden change from 70 nF to 91 nF under open-loop.

needs a very high speed sensor, here we don't optimal this instant. It should be noted that the random instant sudden voltage change in capacitor may cause infinite current to flow through the parallel resonant capacitor. However, this is not a big problem as there are parasitic inductors and resistors on the PCB board that limit the effect of sudden voltage changes on the parallel resonant capacitor C_r'. The second phenomenon is the delay of resonant circuit responses, but in this manuscript, Such a delay is irrelevant. But it is hard to take this four-quadrant switch and auxiliary resonance branch into control loop.

Fig. 11 shows the experiment results of prototype under resonant parameter sudden change from 91 nF to 70 nF under open-loop and its zoom-in waveforms. The delay in

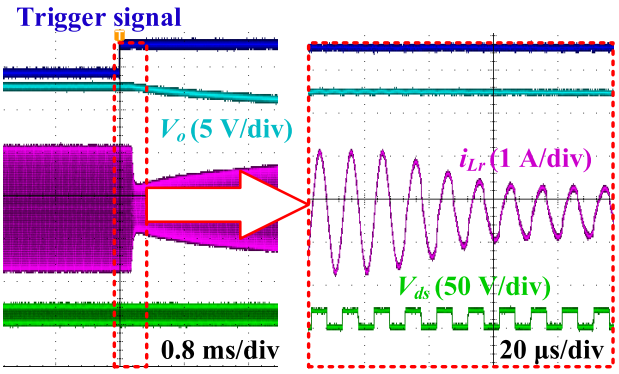

FIGURE 10. Experimental open-loop response when sudden increase of resonant occurs.

the process of turning-OFF the four-quadrant switch has increased, but it's okay as we just want change the resonant tank parameter.

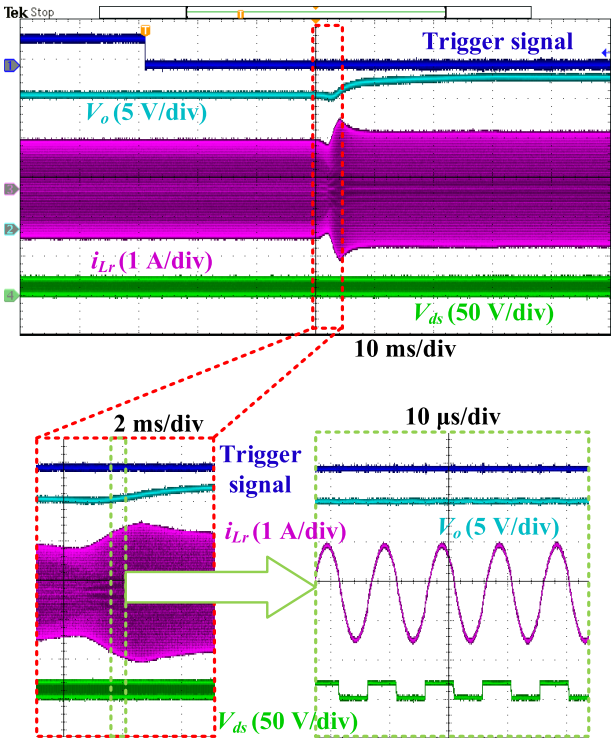

FIGURE 11. Experimental open-loop dynamic response when resonant capacitance steps from 91 nF to 70 nF.

B. EXPERIMENTAL RESULTS

PID control can also be used to regulate the output voltage of an *LLC* converter. In the experiment, a PID controller-based *LLC* converter is tested as the baseline for comparison. In fact, PID control is a commonly used technique for controlling the output of many types of power converters, including *LLC* converters.

PID control is a powerful technique for controlling the output of an *LLC* converter and can help improve the converter's stability and response time. However, tuning a PID controller can be challenging, especially for complex systems like power converters such as the *LLC* converter [25]. The tuning process can be time-consuming and require significant expertise, as the optimal PID gains can depend on various factors, such as the dynamics of the system, the desired response time, and the specific requirements of the application. However, an empirical approach can be used to tune the PID controller based on experimental data. The empirical approach involves adjusting the PID controller gains based on the system's response to a step input. This method first set the proportional gain to a small value, and the integral gains to zero, then apply a step input to the system and record the output response, increase the proportional gain until the output voltage begins to oscillate, and then reduces the gain slightly, add a small amount of integral gain to eliminate any steady-state error.

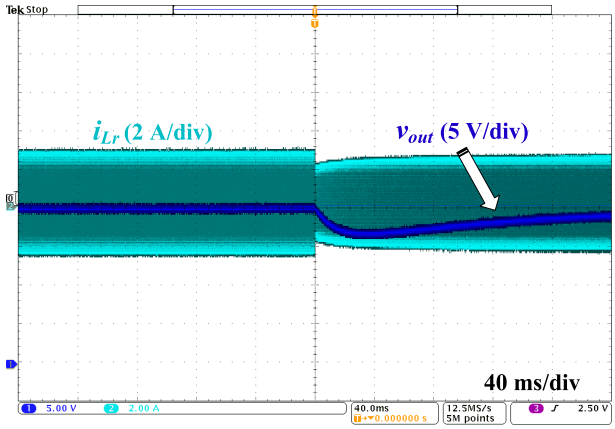

FIGURE 12. Experiment results of the prototype under resonant parameter sudden change from 70 nF to 91 nF and back to normal under PI control.

Fig. 12 shows the experimental results of the prototype under resonant parameter sudden change and back to normal under PI control. The resonant capacitor is changed from 70 nF to 91 nF, resulting in a shift of the resonant frequency from 105 kHz to 91 kHz. When PI control is applied, the switching frequency is gradually adjusted to approach the resonance frequency. The response time for this adjustment is approximately 280ms, and the peak overshoot percentage is about 16.57%. However, due to the non-linear characteristic of the *LLC* converter, the response performance is not as desired.

To demonstrate the effectiveness of the proposed ARFT control scheme, we conduct experiments under various scenarios. One of the experiments involves subjecting the prototype to sudden changes in the resonant parameters, followed by restoring them to their normal values using the fixed-step feedback control described in [14], which can represent a large portion of large-signal methods. This experiment serves as a demonstration of the efficacy of our proposed control scheme. Under this control method, the Δf_s shown in Fig. 5

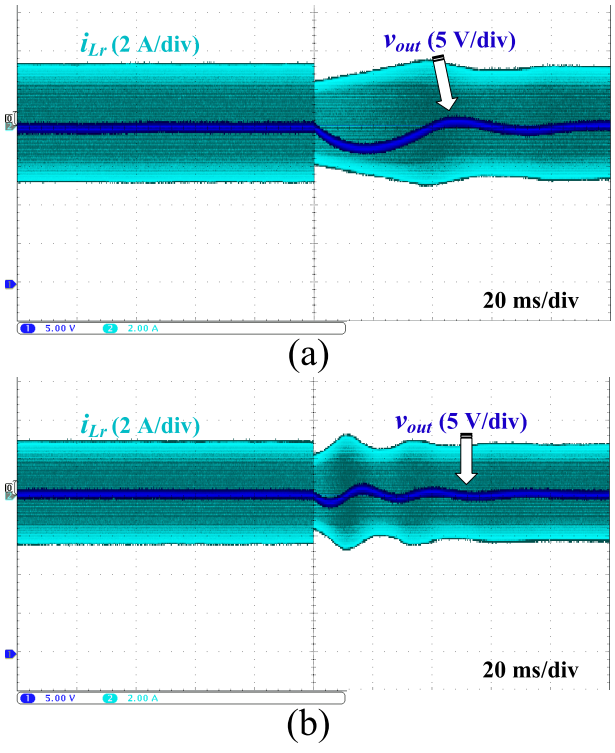

FIGURE 13. Experiment results of the prototype under resonant capacitance sudden drops from 70 nF to 91 nF and back to normal. (a) under fixed-step feedback control and (b) under proposed ARFT control scheme combined with large-signal and small-signal approaches.

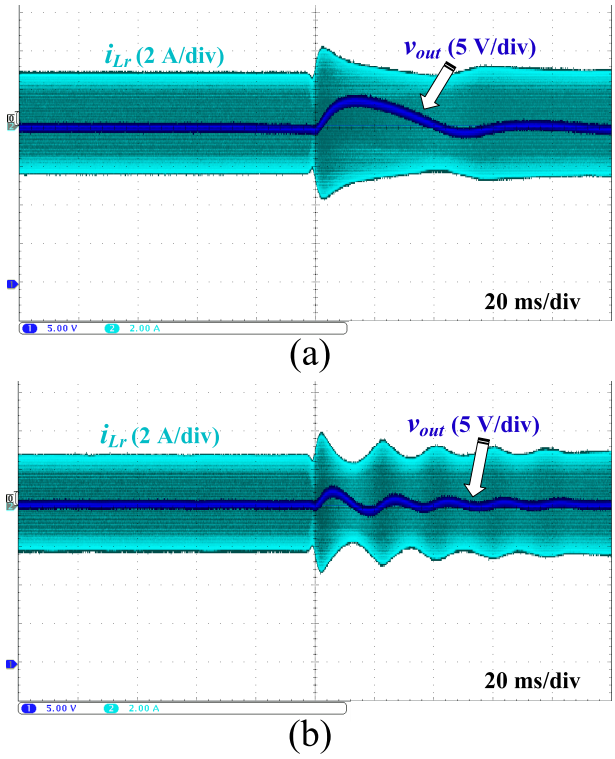

FIGURE 14. Experiment results of the prototype under resonant capacitance sudden increases from 70 nF to 91 nF and back to normal. (a) under fixed-step feedback control and (b) under proposed ARFT control scheme combined with large-signal and small-signal approaches.

is a fixed value. Fig.13 (a) displays the results of this experiment. The resonant capacitor is also changed from 70 nF to 91 nF, causing a shift of the resonant frequency from 105 kHz to 91 kHz. To maintain a stable output voltage, the fixed-step feedback control is applied, and the switching frequency is adjusted to be close to the resonance frequency. The response time for this adjustment is approximately 90ms, and the peak overshoot percentage is about 13.1%. Fig.13 (b) displays the same capacitor change but under proposed ARFT control scheme. The peak undershoot observed is reduced for the proposed ARFT control scheme in comparison to the PI controller and fixed-step feedback controller, which is 4.4%. The response time is also reduced to about 35ms.

Fig.14 (a) shows the experiment results of the *LLC* converter under resonant capacitance sudden change from 91 nF to 70 nF and back to normal under fixed-step feedback control, The response time for this sudden increase is about 80ms, and the peak overshoot percentage is about 18.3%. However, there is still room for improvement in the performance of the system. Fig.14 (b) shows the experiment results of the same capacitor drops and output voltage back to normal under the proposed ARFT control scheme combined with large-signal and small-signal approaches. The response time for the resonant capacitor sudden increase experiment is approximately 45ms, and the peak overshoot percentage is about 8.7%.

Compared with the above control strategy, the proposed ARFT control scheme has superior performance than traditional methods. This means that the converter can achieve a faster and more accurate response to changes in load or input voltage, resulting in improved system stability and efficiency.

Traditional small-signal methods, like those utilized in [12] and [19], necessitate additional current sensors, leading to higher hardware costs.In contrast, the proposed ARFT control scheme achieves comparable performance levels without the need for excessive computing resources or additional sensors. This is a significant advantage as it enables the implementation of the control scheme on low-cost microcontrollers, making it a practical solution for a wide range of applications. Ultimately, the proposed ARFT control scheme enhances the performance of controlling *LLC* resonant converters without compromising affordability or accessibility.

V. CONCLUSION

This manuscript proposes a new ARFT scheme that based on large and small signal combined model which has improved dynamic performance for *LLC* resonant converter. The ARFT scheme has been specially optimized for detecting the resonant frequency by using small-signal model based ESO. One key concept that the output voltage ripple of an *LLC* resonant converter contains information about its resonant frequency,

which can be observed. The controller monitors the voltage gain of the converter, which is the large-signal model approach. By combining these two models, the controller can achieve improved performance in both response time and peak overshoot percentage. The experimental results validate the proposed ARFT scheme for *LLC* resonant converter. It is possible to apply this ARFT scheme in future input-series-output-parallel structure LLC converter.

REFERENCES

[1] D. Ma, W. Chen, and X. Ruan, "A review of voltage/current sharing techniques for series-parallel-connected modular power conversion systems," *IEEE Trans. Power Electron.*, vol. 35, no. 11, pp. 12383–12400, Nov. 2020.
[2] Z. Li, B. Xue, and H. Wang, "An interleaved secondary-side modulated *LLC* resonant converter for wide output range applications," *IEEE Trans. Ind. Electron.*, vol. 67, no. 2, pp. 1124–1135, Feb. 2020.
[3] H. Wen, Y. Liu, D. Jiao, C.-S. Yeh, and J.-S. Lai, "Design principles and optimization considerations of a high frequency transformer in GaN based 1 MHz 2.8 kW *LLC* resonant converter with over 99% efficiency," in *Proc. IEEE Appl. Power Electron. Conf. Expo. (APEC)*, Jun. 2021, pp. 1939–1944.
[4] Z. U. Zahid, Z. M. Dalala, R. Chen, B. Chen, and J.-S. Lai, "Design of bidirectional DC–DC resonant converter for vehicle-to-grid (V2G) applications," *IEEE Trans. Transport. Electrific.*, vol. 1, no. 3, pp. 232–244, Oct. 2015.
[5] Q. Ma, Q. Huang, and A. Q. Huang, "Performance analysis of an input-series-output-parallel *LLC* resonant converter with parameters mismatch," in *Proc. IEEE Energy Convers. Congr. Expo. (ECCE)*, Oct. 2021, pp. 3203–3210.
[6] D. Cittanti, M. Gregorio, E. Vico, F. Mandrile, E. Armando, and R. Bojoi, "High-performance digital multiloop control of *LLC* resonant converters for EV fast charging with LUT-based feedforward and adaptive gain," *IEEE Trans. Ind. Appl.*, vol. 58, no. 5, pp. 6266–6285, Sep. 2022.
[7] F. Degioanni, I. G. Zurbriggen, and M. Ordonez, "Dual-loop controller for *LLC* resonant converters using an average equivalent model," *IEEE Trans. Power Electron.*, vol. 33, no. 11, pp. 9875–9889, Nov. 2018.
[8] H. Wang, S. Dusmez, and A. Khaligh, "Maximum efficiency point tracking technique for *LLC*-based PEV chargers through variable DC link control," *IEEE Trans. Ind. Electron.*, vol. 61, no. 11, pp. 6041–6049, Nov. 2014.
[9] Y. Wei, Q. Luo, and A. Mantooth, "Overview of modulation strategies for *LLC* resonant converter," *IEEE Trans. Power Electron.*, vol. 35, no. 10, pp. 10423–10443, Oct. 2020.
[10] Z. U. Zahid, J. J. Lai, X. K. Huang, S. Madiwale, and J. Hou, "Damping impact on dynamic analysis of *LLC* resonant converter," in *Proc. IEEE Appl. Power Electron. Conf. Expo. (APEC)*, Mar. 2014, pp. 2834–2841.
[11] S. Kapat and P. T. Krein, "A tutorial and review discussion of modulation, control and tuning of high-performance DC–DC converters based on small-signal and large-signal approaches," *IEEE Open J. Power Electron.*, vol. 1, pp. 339–371, 2020.
[12] U. Kundu and P. Sensarma, "A unified approach for automatic resonant frequency tracking in *LLC* DC–DC converter," *IEEE Trans. Ind. Electron.*, vol. 64, no. 12, pp. 9311–9321, Dec. 2017.
[13] S. S. Chakraborty and K. Hatua, "Modeling with beat frequency dynamics and phase-frequency control design for a dual-bridge series resonant converter," *IEEE Trans. Ind. Electron.*, vol. 69, no. 8, pp. 7952–7962, Aug. 2022.
[14] Y. Wei, Q. Luo, and H. A. Mantooth, "A resonant frequency tracking technique for *LLC* converter-based DC transformers," *IEEE J. Emerg. Sel. Topics Ind. Electron.*, vol. 2, no. 4, pp. 579–590, Oct. 2021.
[15] J. Min and M. Ordonez, "Unified bidirectional resonant frequency tracking for CLLC converters," *IEEE Trans. Power Electron.*, vol. 37, no. 5, pp. 5637–5649, May 2022.
[16] A. Awasthi, M. Pahlevani, and P. Jain, "Multi-variable hybrid switching frequency-duty cycle based phase-shift control for DC–DC resonant converters," in *Proc. IEEE Appl. Power Electron. Conf. Expo. (APEC)*, Jun. 2021, pp. 1951–1957.
[17] H. Li and Z. Jiang, "On automatic resonant frequency tracking in *LLC* series resonant converter based on zero-current duration time of secondary diode," *IEEE Trans. Power Electron.*, vol. 31, no. 7, pp. 4956–4962, Jul. 2016.
[18] Y.-S. Lai and M.-H. Yu, "Online autotuning technique of switching frequency for resonant converter considering resonant components tolerance and variation," *IEEE J. Emerg. Sel. Topics Power Electron.*, vol. 6, no. 4, pp. 2315–2324, Dec. 2018.
[19] C. Buccella, C. Cecati, H. Latafat, P. Pepe, and K. Razi, "Observer-based control of *LLC* DC/DC resonant converter using extended describing functions," *IEEE Trans. Power Electron.*, vol. 30, no. 10, pp. 5881–5891, Oct. 2015.
[20] S. Zhuo, A. Gaillard, L. Xu, H. Bai, D. Paire, and F. Gao, "Enhanced robust control of a DC–DC converter for fuel cell application based on high-order extended state observer," *IEEE Trans. Transport. Electrific.*, vol. 6, no. 1, pp. 278–287, Mar. 2020.
[21] R. He, H. Wang, and B. Xue, "Automatic resonant frequency tracking scheme for *LLC* resonant converter based on adaptive extended state observer," in *Proc. IEEE Appl. Power Electron. Conf. Expo. (APEC)*, Mar. 2022, pp. 22–26.
[22] S. Tian, F. C. Lee, and Q. Li, "Equivalent circuit modeling of *LLC* resonant converter," *IEEE Trans. Power Electron.*, vol. 35, no. 8, pp. 8833–8845, Aug. 2020.
[23] J. Zhang, W. X. Zheng, H. Xu, and Y. Xia, "Observer-based event-driven control for discrete-time systems with disturbance rejection," *IEEE Trans. Cybern.*, vol. 51, no. 4, pp. 2120–2130, Apr. 2021.
[24] P. Zhang, J. Wang, Y. Cheng, and S. Jiao, "Reduced-order generalized extended state observer based control for discrete-time systems," in *Proc. Int. Conf. Cyber-Phys. Social Intell. (ICCSI)*, Nov. 2022, pp. 670–675.
[25] J. Han, "From PID to active disturbance rejection control," *IEEE Trans. Ind. Electron.*, vol. 56, no. 3, pp. 900–906, Mar. 2009.

RUNHUI HE (Student Member, IEEE) received the B.S. degree in electrical engineering and automation from the Hefei University of Technology, Hefei, China, in 2020. He is currently pursuing the M.S. degree with the School of Information Science and Technology, ShanghaiTech University, Shanghai, China.

His research interests include LLC resonant converters, solid-state transformer, power balance scheme, and control optimization.

BO XUE (Student Member, IEEE) received the B.S. degree in electrical engineering and automation from the Hefei University of Technology, Xuancheng, China, in 2017. He is currently pursuing the Ph.D. degree with the School of Information Science and Technology, ShanghaiTech University, Shanghai, China.

His research interests include dc–dc converters, inductive power transfer systems, and resonant converters.

MINGDE ZHOU (Student Member, IEEE) received the B.S. degree in automation from Shandong University, Jinan, China, in 2019. He is currently pursuing the Ph.D. degree in electrical engineering with the School of Information Science and Technology, ShanghaiTech University, Shanghai, China. His research interests include wide gain range resonant converters and dc–dc converters.

MINFAN FU (Senior Member, IEEE) received the B.S., M.S., and Ph.D. degrees in electrical and computer engineering from the University of Michigan–Shanghai Jiao Tong University Joint Institute, Shanghai Jiao Tong University, Shanghai, China, in 2010, 2013, and 2016, respectively.

From 2016 to 2018, he was a Postdoctoral Researcher with the Center for Power Electronics Systems (CPES), Virginia Polytechnic Institute and State University, Blacksburg, VA, USA. He is currently an Assistant Professor with the School of Information Science and Technology, ShanghaiTech University, Shanghai. His research interests include megahertz wireless power transfer, high-frequency power conversion, high-frequency magnetic design, and application of wide-bandgap devices. He holds one U.S. patent, seven Chinese patents, and has authored or coauthored more than 80 papers in prestigious IEEE journals and conferences.

JUNRUI LIANG (Senior Member, IEEE) received the B.E. and M.E. degrees in instrumentation engineering from Shanghai Jiao Tong University, Shanghai, China, in 2004 and 2007, respectively, and the Ph.D. degree in mechanical and automation engineering from The Chinese University Hong Kong, Hong Kong, in 2010.

He is currently an Associate Professor with the School of Information Science and Technology, ShanghaiTech University. His research interests include energy conversion and power conditioning circuits, kinetic energy harvesting and vibration suppression, the IoT devices, and mechatronics.

Dr. Liang was a recipient of three best paper awards from the IEEE International Conference on Information and Automation, in 2009 and 2010, and the 2021 International Conference on Vibration Energy Harvesting and Applications. He is the General Chair of the 2nd International Conference on Vibration and Energy Harvesting Applications (VEH), in 2019. He is an Associate Editor of *IET Circuits, Devices and Systems*.

YU LIU (Senior Member, IEEE) received the B.S. and M.S. degrees in electrical engineering from Shanghai Jiao Tong University, Shanghai, China, in 2011 and 2013, respectively, and the M.S. and Ph.D. degrees in electrical and computer engineering from the Georgia Institute of Technology, Atlanta, GA, USA, in 2013 and 2017, respectively.

He is currently a tenure-track Assistant Professor with the School of Information Science and Technology, ShanghaiTech University, Shanghai. His research interests include modeling, protection, fault location, and the state/parameter estimation of power systems, and power electronic systems.

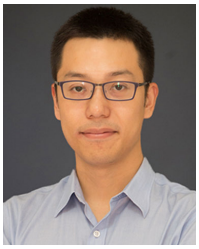

HAOYU WANG (Senior Member, IEEE) received the bachelor's degree (Hons.) in electrical engineering from Zhejiang University, Hangzhou, China, in 2009, and the Ph.D. degree in electrical engineering from the University of Maryland at College Park, College Park, MD, USA, in 2014.

In September 2014, he joined the School of Information Science and Technology, ShanghaiTech University, Shanghai, China, where he is currently a tenured Associate Professor. His research interests include power electronics, plug-in electric and hybrid electric vehicles, the applications of wide-bandgap semiconductors, renewable energy harvesting, and power management integrated circuits.

Dr. Wang is an Associate Editor of IEEE TRANSACTIONS ON INDUSTRIAL ELECTRONICS, IEEE TRANSACTIONS ON TRANSPORTATION ELECTRIFICATION, and *CPSS Transactions on Power Electronics and Applications*. He is also a Guest Editor of IEEE JOURNAL OF EMERGING AND SELECTED TOPICS IN POWER ELECTRONICS.